

Abstract

Velocity Map Imaging Spectroscopy of C₂H⁻ and C₂D⁻: a benchmark study of vibronic coupling interactions

Benjamin A. Laws,^{*†‡} Zachariah D. Levey,[†] John F. Stanton,[¶]

Timothy W. Schmidt,[†] and Stephen T. Gibson[†]

^{*}School of Chemistry, University of New South Wales, Sydney NSW 2052, Australia
[†]Research School of Physics, The Australian National University, Canberra ACT 2601,

Australia

[¶]Department of Chemistry, University of Florida, Gainesville, Florida 32611, United States

E-mail: b.laws@unsw.edu.au

High-resolution velocity map imaged photoelectron spectra of the ethynyl anions C₂H⁻ and C₂D⁻ are measured over a range of photodetachment wavelengths, to investigate the complex interactions between the close lying $\tilde{X}^2\Sigma^+$ and $A^2\Pi$ electronic states. Vibronic coupling calculations are performed by transforming to a quasidiabatic representation, parametrised by *ab initio* CFOUR calculations, to model the interplay between pseudo Jahn-Teller and Raman-Teller coupling. This approach is combined with electron anisotropy measurements to assign all of the observed vibronic structure, providing a framework that may be used to accurately simulate spectra of larger C_nH monohydride carbon chains.

Introduction

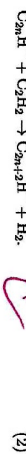
Carbon monohydrides C_nH, are a class of linear radicals that play an important role in combustion and interstellar chemistry.^{1–4} These carbon chains have been observed in many interstellar environments, including planetary atmospheres,^{4–6} comets,⁷ dark clouds,^{8,9} and during heavy star formation.^{10,11} Due to their relatively high abundance in a variety of astronomical conditions, they are believed to be promising candidates for Diffuse Interstellar Band (DIB) carriers.^{9,12–16} The corresponding anions C_nH⁻ are also believed to play an important role in interstellar chemistry.^{9,17} C₆H⁻ was the first negative ion detected in space, after it was observed in two distinct interstellar molecular clouds IRC+10216 and TMC-1 in 2006.¹⁸ More recently, anions C₄H⁻¹⁹ and C₅H⁻^{20,21} have also been detected in a range of environments, include dark clouds,²² prestellar cores,²³ and protostellar envelopes.²⁴

Chain growth of the C_nH radicals occurs predominately through acetylene addition,



Conversely, the formation of anions in space is believed to be driven by radiative electron

attachment, charge transfer, and dissociation electron attachment. Current astrochemical modelling of interstellar clouds, such as IRC+1026, typically underestimate the observed abundances of CH_4^- .^{17,22,25} Therefore, it has been proposed that ion-neutral reactions



may be significant chain growth mechanisms that also needs to be included in astrochemical models.^{17,26} Studies of the extraterrestrial planetary atmosphere of Saturn's moon Titan suggest that both C_2H and C_2H^- play an important role in the atmospheric chemistry.^{6,27–29} Multiple reaction pathways involving the C_2H^- have been proposed, including reactions with C_2H_2 and HCN .

Our knowledge of interstellar chemistry relies critically on theory to provide a link between astronomical observations and terrestrial laboratory studies. Microwave spectroscopy has successfully been used in this fashion to identify a large number of molecules in the interstellar medium (ISM). However for some species, particularly those with low abundances or no dipole moment, UV/vis spectroscopic methods are required for identification.³⁰ This creates a challenge for theory, as electronic spectra calculations are more sensitive to the levels employed than pure rotational spectra.³¹ This becomes even more challenging when vibronic coupling effects are introduced, as they can be exceedingly difficult to model.

These considerations may be explored by examining some of the smallest carbon monohydrides. The ethynyl radical C_2H may appear to be a simple linear triatomic molecule.

However the electronic spectrum is complicated by the presence of the close-lying ground $^2\Sigma^+$ and first excited $^2\Pi$ surfaces, which are only separated by $\sim 3,700 \text{ cm}^{-1}$.^{32,33} The interaction of these surfaces produces a complex vibronic spectrum around the $A^2\Pi$ state, where the $\tilde{X} - \tilde{A}$ origin is spread over multiple admixed vibronic levels. In C_4H the $^2\Sigma^+$ and $^2\Pi$ states are nearly degenerate, resulting in even stronger couplings,³⁴ while in C_6H and C_8H the ordering of the states swaps, with a ground $^2\Pi$ state and a low lying excited $^2\Sigma^+$

dissociative

seen quite quickly

state.^{35,36} Consequently, understanding the vibronic coupling interactions between the $^2\Sigma$ and $^2\Pi$ surfaces will be essential in order to accurately model the role these radicals (and their corresponding anions) are likely to play in the interstellar chemistry mentioned above,

and to guide the search for possible DB carriers.

In this paper we study the vibronic spectrum of the ethynyl radical C_2H by employing High-Resolution Photoelectron Imaging (HR-PEI) ~~to set the benchmark~~ CPOUR³⁷ ~~ab initio~~ vibronic-coupling calculations. C_2H is reported to be one of the most abundant molecules in the universe, and is the most thoroughly studied of the C_nH species.^{3,31,38} Many different experimental techniques have been employed to try and resolve the complex vibronic spectrum, including electron spin resonance,^{39,40} laser magnetic resonance,^{41–43} microwave and millimeter wave spectroscopy,^{44–47} infrared (matrix isolation,^{48–50} and Fourier Transform emission⁵¹) spectroscopy, laser induced fluorescence spectroscopy^{52–54} and photo-electron spectroscopy.^{34,36,35} C_2H has also received extensive theoretical attention to try and understand the experimental results, however the large number of possible vibronic levels means this has proven to be a challenge.^{31,33,36–43} In this work we demonstrate how construction of a quasidiabatic Hamiltonian allows for the strength of vibronic interactions between coupled surfaces near a conical intersection to be estimated, in order to stimulate electronic and vibronic spectra. By employing anion HR-PFI both the $^2\Sigma^+$ and $^2\Pi$ surfaces are mapped out on an equal footing from the anion $\tilde{X}^+\Sigma^+$ state, allowing for direct comparison to the *ab initio* modelling.

Results and Analysis

Ethyne ions were produced in a pulsed-jet discharge of pure C_2H_2 gas, and subsequently mass isolated via time of flight. Electrons were detached using a tuneable Sunlike Optical Parametric Oscillator (OPO) pumped with the third harmonic of a Nd:YAG laser. High electron counts could also be obtained by using the third and fourth harmonics of the Nd:YAG

laser directly. The detached electrons were then mapped onto a micro channel plate detector using a Velocity Map Imaging (VMI) lens. An illustrative VMI of ~ 4 million electrons collected from 355 nm (3.49 eV) photodetachment of C_2H^- is shown in Fig. 1(a). The electrons are distributed radially according to their speed, with slow electrons at the image center, and fast electrons located towards the outer edge. Due to the relatively large C_2H^- electron affinity (EA) of 2.969 eV, ss photodetachment at 355 nm occurs close to threshold. This yields slow electrons, allowing for a low repeller voltage (~ 600 V) on the VMI lens, and high velocity resolution.

Despite being close to threshold, two electronic states of neutral C_2H are observed. The faster electrons on the outer edge correspond to $\text{C}_2\text{H}(\tilde{\chi}^2\Sigma^+) + e^- \rightarrow \text{C}_2\text{H}^-(\tilde{\chi}^2\Sigma^+) + h\nu$ photodetachment, and are preferentially distributed around the poles of the image, indicative of a positive anisotropy parameter. Conversely the angular distribution of the slower electrons near the center are skewed towards the equator, indicative of a negative anisotropy parameter. These electrons may be assigned to photodetachment to the first excited state $\text{C}_2\text{H}(\tilde{A}^2\Pi) + e^- \rightarrow \text{C}_2\text{H}^-(\tilde{\chi}^2\Sigma^+) + h\nu$.

To investigate the vibronic coupling interaction between these two nearby Σ^+ and Π surfaces, deuterated ethyryl C_2D^- was also studied. C_2D^- ions were produced in a discharge of pure C_2D_4 gas and measured under the same experimental conditions as C_2H^- . An illustrative VMI of photodetachment at 355 nm from C_2D^- is shown in Fig. 1(b). Similarly to Fig 1(a) two electronic transitions are observed. While the fast electrons appear similar in both images, a striking difference is observed in the slow electrons near the detector center. In Fig. 1(a) a series of weak rings are observed, however in Fig. 1(b) the image is dominated by two distinct rings.

The VMIs in Fig. 1 were inverted using the Abel inversion methods detailed in pyAbel,⁶⁴ to extract the corresponding photoelectron spectra presented in Fig. 1(c). Below 27,000 cm⁻¹ on the $\tilde{\chi}^2\Sigma^+$ surface the C_2H^- and C_2D^- spectra are a close match. Both are dominated by the origin transition, shifted by ~ 10 cm⁻¹ in the deuterated spectrum, with progressions

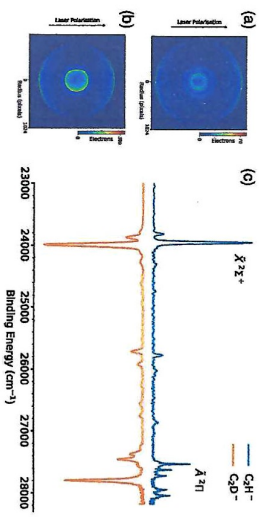


Figure 1: (a) A 3D-representation of the velocity-map image of ~ 4 million photoelectrons detached from C_2H^- at 355 nm. The outer rings, distributed around the vertical laser polarisation axis, represents photodetachment to the ground $\tilde{\chi}^2\Sigma^+$ state. The inner rings represent detachment to the first excited state $\tilde{A}^2\Pi$. (b) Photoelectron spectra of C_2H^- at 355 nm showing intensity profiles versus binding energy, illustrating the change in electron intensity profile and energy resolution.

involving the $v_2(\pi)$ bending and $v_3(\sigma)$ CC stretch vibrational normal modes. This includes transitions involving an odd quanta of v_2 bending excitation ($2m+1$) which should be totally forbidden within the ~~Hartree-Fock~~⁶⁵ approximation. However, the presence of these transitions in the spectra is ~~likely~~ an indicator of Herzberg-Teller (HT) vibronic coupling between the ground $^2\Sigma^+$ and nearby excited $^2\Pi$ electronic surfaces, as

$$\Sigma^+ \otimes \pi = \Pi. \quad (3)$$

Above 27,000 cm⁻¹, near the $\tilde{A}^2\Pi$ state origin, large differences are observed between the C_2H^- and C_2D^- photoelectron spectra. In the C_2H spectrum 5 sharp peaks are observed, spaced by ~ 95 cm⁻¹. However in the deuterated spectrum, one dominant peak is observed at 27,792 cm⁻¹, with 3 weaker peaks centred around 27,360 cm⁻¹. Unlike the structure below 27,000 cm⁻¹ none of these peaks are able to be readily assigned to vibronic transitions, due to the presence of strong coupling interactions between the nearby Σ^+ and Π surfaces.

Premissibly features
vibronic features
both in states
in the antisymmetry
exhibit the 'other'
exhibit the 'other'
symmetry

Vibronic Coupling Interactions

The complex spectral structure observed near the $\tilde{A}^2\Pi$ state origin in Fig. 1(c) may be understood by considering the v_2 bending vibrational mode. To account for the degeneracy of this mode, the vibronic quantum number ℓ_i may be introduced, representing the angular momentum associated with the bending motion. This may take a value of $\ell_i = v_i, v_i - 2, v_i - 4, \dots, 1$ or 0, where v_i is the quanta of bending excitation. In the Born-Oppenheimer approximation different vibronic energy levels ℓ_i are degenerate, however in cases with strong rovibronic coupling, this degeneracy in ℓ_i is lost.

In C₂H this effect creates a Renner-Teller (RT) pair in the excited state, where the usually degenerate II surfaces separate to form two non-degenerate electronic states $\Pi^+(2A')$ and $\Pi^-(1A'')$. This involves separating a single potential energy surface (V) into two distinct but connected surfaces (V^+) and (V^-). Due to the strong coupling along the linear axis between the electronic and vibration angular momenta of the $2A'$ and $1A''$ components of the $\Sigma\Pi$ state, stationary states cannot be explicitly assigned to either of the $\Pi^+(2A')$ or $\Pi^-(1A'')$ electronic surfaces. Instead, they exist as a combination of both states.

Due to the close lying nature of the ground $\tilde{X}^2\Sigma^+$ and excited $\tilde{A}^2\Pi$ electronic states, which are only separated by ~ 3700 cm⁻¹, a pseudo Jahn-Teller effect is also observed. In the case of C₂H this is seen as coupling between the ground $\Sigma^+(1A')$ and excited $\Pi^+(2A')$ states, induced by the bending motion of v_2 . The ground state only couples to one of the Renner-Teller pair $\Pi^+(2A')$, as the other state $\Pi^-(1A'')$ has incorrect symmetry. This results in the complex vibronic structure observed for the $\tilde{A}^2\Pi$ electronic state, with contributions from three coupled surfaces $\Sigma^+(1A')$, $\Pi^+(2A')$, and $\Pi^-(1A'')$.

These interactions spread the electronic origin of the $\tilde{A}^2\Pi$ state over several vibronic levels. Therefore, instead of assigning a defined origin, the observed peaks in the spectrum may be assigned to coupled admixtures of vibronic transitions involving the three potential

energy surfaces,

$$\Psi_f = \sum_{\xi} \psi_{\xi}^f \sum_k C_{jk}^{\xi} \phi_{j,m}^{\xi}, \quad (4)$$

where ψ_{ξ}^f is the diabatic electronic wavefunction, and $\phi_{j,m}^{\xi}$ is the spin-rovibrational wavefunction. ξ represents the electronic states used in the expansion ($\xi = \Sigma^+(1A')$, $\Pi^+(2A')$, $\Pi^-(1A'')$). A depiction of these three interacting surfaces is given in Fig. 2.

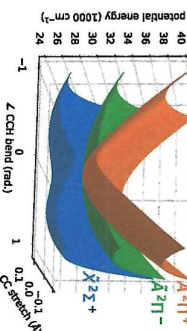


Figure 2: Adiabatic potential energy surfaces of $\tilde{X}^2\Sigma^+$, $\tilde{A}^2\Pi$, and $\tilde{A}^2\Pi^+$ states, calculated using the method developed by Tarroni and Carter³³ ($E_{1A'}$, $E_{2A'}$, and $E_{1A''}$ in Eq. 4).

The adiabatic potential energy surfaces in Figure 2 were calculated using the variational method of Tarroni and Carter.³¹ This has been used to calculate a multitude of admixed vibronic levels. In the literature, over 100 possible C₂H vibronic states have been calculated, up to 10,000 cm⁻¹ above the $\tilde{X}^2\Sigma^+$ origin. However, assigning experimental spectra has remained a challenge, partly due to the large number of calculated levels providing multiple possible assignments for each experimentally observed transition.

Coupling Calculations

In order to guide spectral assignment of C₂H and astronomical searches for other C₂H radicals, transition intensities are also needed. However, due to the strong vibronic coupling interactions, this can not be obtained via standard quantum chemistry methods. To account for these interactions, the photoelectron spectrum of the C₂H- anion was simulated using a quasidiabatic Hamiltonian of the type advocated by Koepel, Domke and Cederbaum

I think that Pizzinelli + Carter (a year or so later) single Franck-Condon said based on Carter's "definitive" work is the here . . .

(KDC).^{65,66} In this approach, the Hamiltonian is represented in a basis of quasidiabatic (slowly varying) electronic states for which the kinetic energy operator can be assumed diagonal.⁶⁷ For C₂H, the KDC Hamiltonian comprises three states - the two components of the ² Π state and the ground ² Σ^+ state - and is then projected onto a vibrational basis, usually chosen as a direct product of harmonic oscillators. Diagonalization of the corresponding matrix yields the molecular states (which are given in terms of a Born-Huang expansion), and the squared projections of the corresponding eigenvectors onto the ground state of the anion yield the relative intensities. The latter is ~~approximately~~ true if the photodetachment cross sections for the ² Σ^+ and ² Π states are assumed equal, but different cross sections of the two states can be incorporated by scaling the intensities of states according to their (vibronic) symmetry.⁶⁸

Details of the construction and parametrization of KDC Hamiltonians can be found elsewhere in the literature,^{68,69-72} and the procedure followed will be discussed here only briefly. The present calculations use the so-called quadratic vibronic coupling (QVC) model.⁶⁹ For the system at hand, the QVC model Hamiltonian assumes the following form

$$H = T_n \mathbf{1} + V, \quad (5)$$

$$\begin{aligned} X &= \begin{pmatrix} \Delta_0^X + F_{22}^X + F_{22}^A q_{22} & \lambda q_{2a} & \lambda q_{2b} \\ \frac{1}{2} \sum_{ab} F_{22}^A q_a q_b & \Delta_0^A + F_{22}^A q_{2a} + F_{22}^X q_{2b} & \eta q_{2a} q_{2b} \\ \lambda q_{2a} & \eta q_{2a} q_{2b} & \Delta_0^A + F_{22}^A q_{2a} + F_{22}^X q_{2b} \\ \lambda q_{2b} & \eta q_{2a} q_{2b} & \frac{1}{2} \sum_{ab} F_{22}^A q_a q_b - \frac{1}{2} \sum_{ab} F_{22}^X q_a q_b \end{pmatrix} \quad (6) \end{aligned}$$

where the summations run over the dimensionless normal modes (q_i) that serve as the coordinate system for the problem.^{61,68} For convenience, the latter are chosen to be those of the anion, which considerably facilitates calculation of the spectral intensities. In Eq. (6),

the diagonal terms of V (excluding those that carry the Renner-Teller coupling constant η) represent the quasidiabatic potential energy surfaces of the ² Σ^+ and the two components of the ² Π state, chosen here as those in which the unpaired electron lies within or is perpendicular to an arbitrarily chosen plane, designated as A(a') and A(a''), respectively. Δ_0^X is the separation of the anion and ² Σ^+ states at the origin of the coordinate system (the vertical electron detachment energy), and Δ_0^A is the gap between anion and ² Π states at the same geometry.

For the modes of σ symmetry (q_1 and q_2), the diabatic forces (F_i) and force constants (F_{ij}) coincide with those of the adiabatic potential energy surfaces. However, for the bending mode, the diabatic (F_{22}) and adiabatic (f_{22}) force constants differ, and the parametrization is somewhat more involved. For each component of the ² Π state, either the 2a or 2b component of the bending vibration will maintain the A' electronic symmetry that is needed to couple with the ² Σ^+ state. Designating these as 2a for the A(a') state and 2b for the A(a'') state (as is implicit in Eq. 6), the diabatic force constants for the bending mode in the ² Σ^+ and ² Π states can be written as

$$F_{22}^X = f_{22}^X + \frac{2\lambda^2}{(\Delta_0^A - \Delta_0^X)} \quad (7)$$

$$F_{22}^A = f_{22a}^{A(C)} - \frac{2\lambda^2}{(\Delta_0^A - \Delta_0^X)} - \eta \quad (8)$$

where the Renner-Teller interaction strength (η) is determined from

$$\eta = \frac{1}{2} \left[f_{22a}^{A(C)} - f_{22b}^{A(C)} - \frac{2\lambda^2}{(\Delta_0^A - \Delta_0^X)} \right] \quad (9)$$

once the interstate coupling (λ which is calculated analytically in this work, see below) is known.

When the potential in Eq. (6) is diagonalized, the adiabatic states that are used for its parametrization are precisely recovered through terms second order in displacement. The

Linear diabatic coupling constants between the electronic states of interest were calculated analytically at the EOM-CCSDT/AN02 level of theory, using the CFOUR computational package³⁷ and the quasidiabatic ansatz of Iohino *et al.*⁷¹ Briefly, the EOM procedure is used to operationally define quasidiabatic states (those that relax according to a well-behaved reference state wavefunction), and the coupling constants are then evaluated as the first derivative of the off-diagonal elements of the electronic Hamiltonian in the basis defined by this representation. The diabatic force and coupling constants calculated to parametrize the KDC potential in Eq. (6) are presented in Table 1.

Table 1. Parameters for the quasidiabatic Hamiltonian Eq. (6) determined using CFOUR and the quasidiabatic ansatz.  Give unit

parameter	C_2H		$\tilde{A}^2\Sigma^+$		$\tilde{A}^2\Pi(g)$		$\tilde{A}^2\Pi(a')$		$\tilde{A}^2\Pi(g'')$		$\tilde{A}^2\Pi(a''')$	
	Anion	$\tilde{X}^2\Sigma^+$	$\tilde{A}^2\Pi(g)$	$\tilde{A}^2\Pi(a')$	Anion	$\tilde{X}^2\Sigma^+$	$\tilde{A}^2\Pi(g)$	$\tilde{A}^2\Pi(a')$	Anion	$\tilde{X}^2\Sigma^+$	$\tilde{A}^2\Pi(g)$	$\tilde{A}^2\Pi(a')$
f1	0	22451.21	26543.67	26543.67	0	22431.21	26533.67	26533.67	0	22431.21	26533.67	26533.67
f2	0	-596.04	641.6	641.6	0	-596.04	641.6	641.6	0	-596.04	641.6	641.6
f3	0	-1515.21	1257.07	1257.07	0	-1401.53	1115.17	1115.17	0	-1401.53	1115.17	1115.17
f4	0	0	0	0	0	0	0	0	0	0	0	0
f11	3424.32	3487.03	3482.16	3482.16	2611.42	2636.57	2681.25	2681.25	2611.42	2636.57	2681.25	2681.25
f12	0.00	-28.32	31.46	31.46	0.00	-48.38	55.40	55.40	0.00	-48.38	55.40	55.40
f22	1894.71	1830.83	2099.57	2042.21	1792.49	1747.62	1914.39	1914.39	1792.49	1747.62	1914.39	1914.39
f33	607.09	87.57	1883.48	658.96	481.89	1201.09	1503.88	473.55	1201.09	481.89	1503.88	473.55
f44	607.09	87.57	1883.48	658.96	481.89	1201.09	1503.88	473.55	1201.09	481.89	1503.88	473.55
λ	-1185.26	770.7791	-429.4981	-1014.58	770.7791	-429.4981	-1014.58	770.7791	-429.4981	-1014.58	770.7791	-429.4981

Method to calculate the rest

The above method was employed to simulate the photoelectron spectrum of C_2H^- , with the calculated transitions shown in Figure 3(a) alongside the experimental data at 355 nm. On the $\tilde{X}^2\Sigma^+$ surface, below 3,600 cm⁻¹, there is excellent agreement in both the transition positions and intensities between the simulated and experimental spectra. This includes the HT coupled (2^{n+1}) transitions with II symmetry, which would normally be missing from a simulation using standard *ab initio* approaches.

What was CSDT (only)

11

Do really understand? Have calculator.

12

This shall show up in the anisotropy plot? ...

!!! Analytic not yet CCSDT or ANO1/AN01

The positions of the calculated levels for the $\tilde{A}^2\Pi$ state have been shifted by 1,220 cm⁻¹ to account for the EOMIP-CCSDT calculations overestimating the effective Term energy. The experimental data shows that the electronic coupling interactions induce a splitting of the $\tilde{A}^2\Pi$ state origin over 5 vibronic levels, spaced by ~ 95 cm⁻¹ ($a - e$). This splitting is also observed in the calculated spectrum, which correctly predicts 5 prominent transitions in this region. The relative intensities between the calculated transitions are also in good agreement with the experimental data. Peak *d* is slightly underestimated; however, the relative intensity difference between peaks *d* and *e* may be partly explained by the Wigner threshold law,⁷³ which will reduce the intensity of peak *e* in the experimental spectrum as it is close to the detachment threshold. The simulated spectrum also slightly underestimates the splitting between the vibronic levels, which may be linked to the overestimation of the gap between the $\tilde{\Sigma}$ and $\tilde{\Pi}$ surfaces.

The photoelectron spectrum of C_2D^- was also examined using the same approach, with the calculated transitions shown in Figure 3(b) alongside the 355 nm experimental data. Again, there is excellent agreement in the intensity and calculated positions of the transitions on the $\tilde{X}^2\Sigma^+$ state surface, including the HT coupled levels. Near the $\tilde{A}^2\Pi$ state origin, deuteration has a large impact on the experimental photoelectron spectrum. Instead of the evenly split levels observed in C_2H , a single dominant peak (*a*) is now observed at 3,844 cm⁻¹ alongside a collection of weaker peaks (*a - c*) centred around 3,400 cm⁻¹. Based on previous spin-orbit splitting measurements, peak *d* is expected to have significant $\tilde{A}^2\Pi$ character, with peaks *a-c* commonly assigned to vibronic levels with predominantly HT coupled $\tilde{X}^2\Sigma^+$ character.^{53,54,74,75} This suggests that deuteration effectively dampens the coupling interaction between the surfaces.

Like the experimental spectra, a large change is observed in the simulated spectrum upon deuteration. The calculated intensity pattern of the vibronic levels around the $\tilde{A}^2\Pi$ origin is a good match to the experimental data, with a single intense transition observed near peak *d*, and 3 prominent transitions predicted around the experimental peaks *a - c*. The

somewhat shocking but we know now

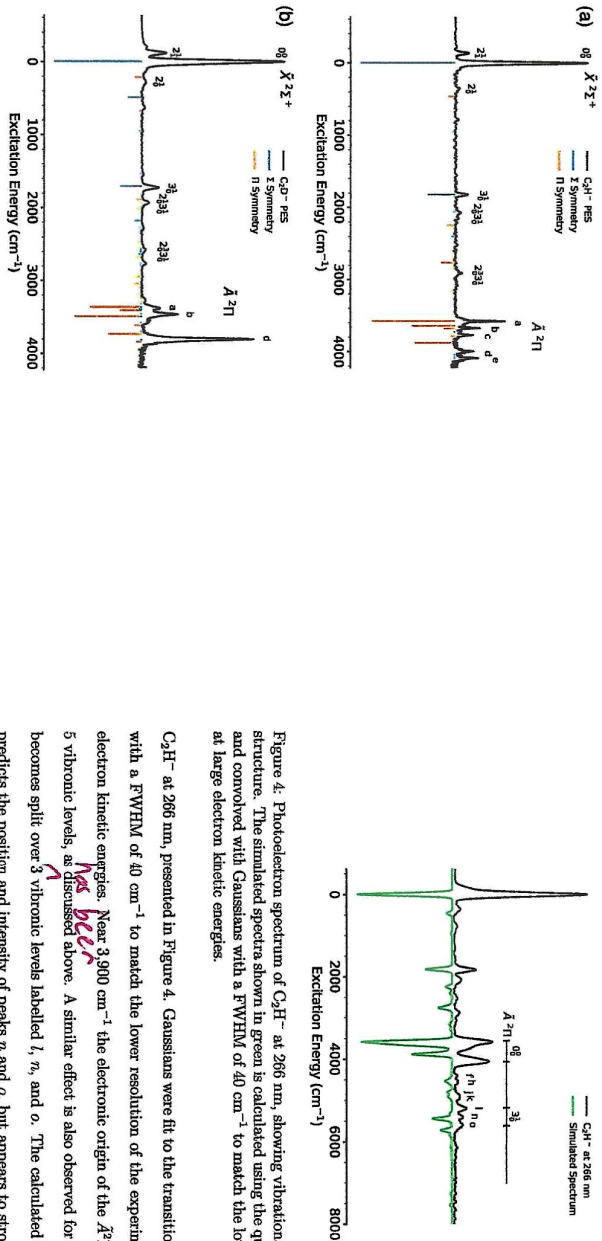


Figure 4: Photoelectron spectrum of C_2F^- at 266 nm, showing vibrationally excited \tilde{A} state structure. The simulated spectra shown in green is calculated using the quasidiabatic ansatz, and convolved with Gaussians with a FWHM of 40 cm^{-1} to match the lower VMI resolution at large electron kinetic energies.

Figure 3: (a) Experimental photoelectron spectrum of C_2H^- at 355 nm, compared to the simulated spectrum calculated using the quasidiabatic ansatz. Transitions with Σ symmetry are shown in blue, transitions with Π symmetry are shown in orange. (b) Experimental photoelectron spectrum of C_2D^- at 355 nm, compared to the simulated spectrum. The labelling of peaks near the A origin correspond to Table SI.

calculated splitting between the levels is also similar, however the relative intensity of peak d appears to be slightly underestimated.

To investigate the effects of coupling on the higher excited vibronic levels on the $\tilde{A}'\Pi$ surface, the calculations were also compared to the experimental photoelectron spectrum of

C_2H^- at 266 nm, presented in Figure 4. Gaussians were fit to the transitions from Figure 3(a) with a FWHM of 40 cm^{-1} to match the lower resolution of the experimental data at high electron kinetic energies. Near 3,900 cm^{-1} the electronic origin of the $\tilde{A}'\Pi$ state is split over 5 vibronic levels, as discussed above. A similar effect is also observed for the 3_0^1 band, which becomes split over 3 vibronic levels labelled l , m , and o . The calculated spectrum correctly predicts the position and intensity of peaks n and o , but appears to strongly underestimate the intensity of peak l . Between the 0_0^0 and 3_0^1 bands a collection of weaker peaks are also observed ($j - k$). These are assigned to highly excited HT coupled $\tilde{X}'\Sigma^+$ transitions (j, k), admixed $\tilde{X} - A$ transitions (h, i) and pure $\tilde{X}'\Sigma^+$ transitions (f). Consequently, peak f will possess Σ symmetry, and should have a different anisotropy to all of the other dominant transitions above 3,800 cm^{-1} . The position and intensity of these highly-excited coupled transitions are well described by the simulated spectrum.

The results from Figures 3 and 4 confirm that the quasidiabatic approach is able to accurately describe the vibronic interactions between the $^2\Sigma^+$ and $^2\Pi$ surfaces, including

deuterium effects. This validates the proposed vibronic interactions, and demonstrates how this method can be employed to decode and assign even complex spectra. Applying this approach to similar less-studied systems will produce reliable predictions for the position and intensity of dominant transitions, which will help guide the search for these molecules in laboratory experiments and astronomical observations.

Photoelectron Angular Distributions

Symmetry considerations may be employed to verify the spectral assignments from the calculations above. The quasidiabatic Hamiltonian approach is able to determine the symmetry of each individual vibronic state, either Σ or Π , which may be compared directly to the experimental electron anisotropy of each transition. The VMIs from this work (Figure 1) were obtained using a linearly polarized detachment laser. Therefore, the differential cross section of emitted electrons is given by

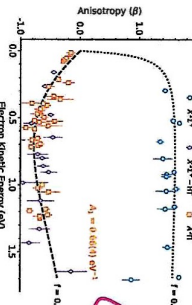
$$\frac{d\sigma}{d\Omega} = \sigma_{\text{total}}[1 + \beta P_2(\cos\theta)], \quad (10)$$

where θ is the angle between the ejected electron and the (vertical) laser polarization, and P_2 is the second-order Legendre polynomial. The anisotropy parameter β provides a quantitative measure of the anisotropy, and can range from -1 to +2 for purely perpendicular and parallel transitions, respectively. Through conservation of angular momentum, β may be described in terms of the detachment partial waves, which are linked to the symmetry of the present detachment orbital. This is discussed in detail elsewhere,^{76,77} and will be only briefly described for the case of C₂H⁻ here.

Photodetachment to the ground state of C₂H ($\tilde{\chi}^2\Sigma^+$) involves ejecting an electron from an s -like $5s_g$ orbital, whereas detachment to the excited $\tilde{A}^2\Pi$ state occurs from a p -like $1p_u$.

state accessed by photo detachment

Figure 5: Photoelectron anisotropy parameters measured for each resolved C₂H⁻ transition, across a range of detachment wavelengths. Allowed ground state transitions $\tilde{\chi}$ are shown in orange. Herzberg–Harter coupled transitions are shown in purple, and excited state transitions \tilde{A} are shown in blue. Anisotropy curves for a mixed- sp model (Eq. 11) are shown for $f=0.1$ and $f=0.9$.



C. Simard
T. Leblanc
J.F. Strobl
TPCL ca.
2012

Figure 5: Photoelectron anisotropy parameters measured for each resolved C₂H⁻ transition, across a range of detachment wavelengths. Allowed ground state transitions $\tilde{\chi}$ are shown in orange. Herzberg–Harter coupled transitions are shown in purple, and excited state transitions \tilde{A} are shown in blue. Anisotropy curves for a mixed- sp model (Eq. 11) are shown for $f=0.1$ and $f=0.9$.

$$\beta(\epsilon)_{\text{sp}} = \frac{2Z\epsilon + 2A_1\epsilon^2 - 4\epsilon \cos\delta_{\pm 1}}{A_1 + 2A_1\epsilon^2 + Z\epsilon} \quad (11)$$

where ϵ is the electron kinetic energy, A_1 is the $s \rightarrow p$ Haustorp coefficient, f is the percentage of p orbital character,

$$Z = \frac{1-f}{f} \frac{8}{3} \quad \text{and} \quad |\psi\rangle = \sqrt{1-f}|s\rangle + \sqrt{f}|p\rangle. \quad (12)$$

From Eq. (11) it can be seen that detachment from a pure s orbital will have a positive anisotropy ($\beta = +2$), whereas detachment from a pure p orbital will have a negative anisotropy for electron kinetic energies $\epsilon < 2/A_1$. Therefore, measuring the anisotropy will determine the electronic character of each individual transition, which may be compared to the calculated symmetries in Figure 3. The anisotropy parameters were measured for every detachment wavelength and prominent transition in the C₂H⁻ photoelectron spectra from this work, and are presented in Figure 5. Fitting Eq. (11) to the anisotropy parameters from $\tilde{\Pi}$ state detachment, with $f=0.9$ produces a Haustorp coefficient of $A_1=0.66(4)$ eV⁻¹.

an s -like $5s_g$ orbital, whereas detachment to the excited $\tilde{A}^2\Pi$ state occurs from a p -like $1p_u$.

state accessed by photo detachment

